THE JOURNAL OF BIOLOGICAL CHEMISTRY VOL. 286, NO. 25, pp. 22160–22169, June 24, 2011

Rescue of Aberrant Gating by a Genetically Encoded PAS (Per-Arnt-Sim) Domain in Several Long QT Syndrome Mutant Human *Ether-á-go-go*-related Gene Potassium Channels*[S]

Received for publication, November 23, 2010, and in revised form, April 29, 2011 Published, JBC Papers in Press, May 2, 2011, DOI 10.1074/jbc.M110.205948

Elena C. Gianulis[‡§] **and Matthew C. Trudeau**[§1]

From the [‡]*Program in Molecular Medicine and* [§]*Department of Physiology, University of Maryland School of Medicine, Baltimore, Maryland 21201*

Congenital long QT syndrome 2 (LQT2) is caused by loss-of-function mutations in the human *ether-á-go-go*-related gene (hERG) voltage-gated potassium (K^+) channel. hERG channels have slow deactivation kinetics that are regulated by an N-terminal Per-Arnt-Sim (PAS) domain. Only a small percentage of hERG channels containing PAS domain LQT2 mutations (hERG PAS-LQT2) have been characterized in mammalian cells, so the functional effect of these mutations is unclear. We investigated 11 hERG PAS-LQT2 channels in HEK293 cells and report a diversity of functional defects. Most hERG PAS-LQT2 channels formed functional channels at the plasma membrane, as measured by whole cell patch clamp recordings and cell surface biotinylation. Mutations located on one face of the PAS domain (K28E, F29L, N33T, R56Q, and M124R) caused defective channel gating, including faster deactivation kinetics and less steady-state inactivation. Conversely, the other mutations caused no measurable differences in channel gating (G53R, H70R, and A78P) or no measurable currents (Y43C, C66G, and L86R). We used a genetically encoded hERG PAS domain (NPAS) to examine whether channel dysfunction could be corrected. We found that NPAS fully restored wild-type-like deactivation kinetics and steady-state inactivation to the hERG PAS-LQT2 channels. Additionally, NPAS rescued aberrant currents in hERG R56Q channels during a dynamic ramp voltage clamp. Thus, our results reveal a putative "gating face" in the PAS domain where mutations within this region form functional channels with altered gating properties, and we show that NPAS is a general means for rescuing aberrant gating in hERG LQT2 mutant channels and may be a potential biological therapeutic.

Congenital Long QT Syndrome (LQTS)[2] is a disorder of the electrical system of the heart characterized by delayed cardiac repolarization that can lead to arrhythmias, syncope, and sudden death (1). Type 2 LQTS (LQT2) is caused by genetic mutations in the human *ether-á-go-go*-related gene (hERG) (2–5). hERG encodes the major subunit of the rapidly activating delayed-rectifier potassium current (I_{Kr}), which plays an essential role in the final repolarization of the ventricular action potential (3, 4). hERG exhibits characteristic slow closing (deactivation) kinetics that are regulated by an N-terminal Per-Arnt-Sim (PAS) domain, which help to specialize the channels for their role in the heart (3, 6–10).

Loss of hERG function, and thus, loss of I_{Kr} (11), can occur through a number of mechanisms, including defects in channel opening and closing (gating), ion permeation, or protein trafficking (12). hERG channels containing LQT2 mutations in the PAS domain (hERG PAS-LQT2) exhibit robust currents when studied in *Xenopus* oocytes (6, 13–15); however, most channels with LQT2 mutations located outside the PAS domain do not have measurable currents and show defects in maturation and trafficking when studied in mammalian cells (12, 16–21). As only 5 hERG PAS-LQT2 channels have been functionally characterized in mammalian cells (20–24), the mechanism for how PAS domain mutations disrupt hERG function when expressed in more physiological conditions remains unclear.

Previously, we showed that slow deactivation could be restored in LQT2 mutant hERG R56Q channels by application of a genetically encoded PAS domain (NPAS) in *Xenopus* oocytes (15). Here, we sought to determine whether NPAS was a general mechanism for rescue of LQT2 mutant channels. To carry out this goal we investigated 1) whether 11 different hERG PAS-LQT2 mutations that were gating deficient in *Xenopus* oocytes resulted in a loss-of-function in a human heterologous expression system and 2) whether NPAS could restore gating in several different hERG PAS-LQT2 mutant channels with gating defects in a mammalian system.

We found that the 11 hERG PAS-LQT2 channels exhibited a spectrum of deficiencies in mammalian cells, and only channels with mutations located on one face of the PAS domain were gating deficient. These mutant channels exhibited an array of gating defects, including faster deactivation kinetics and a right-shift in the steady-state inactivation relationship, the combination of which resulted in aberrant currents in response to a dynamic ramp clamp. We found that NPAS rescued gating defects in hERG PAS-LQT2 channels by inducing slower deactivation kinetics and a left-shift in the steady-state inactivation relationship, which restored wild-type-like currents during the dynamic ramp clamp. Thus, NPAS restored function to channels that had a variety of gating defects. Therefore, in this study,

* This work was supported, in whole or in part, by National Institutes of Health Grants HL-083121 (to M. C. T.) and T32-GM 008181 (to E. C. G.) and a gift from the Helen Pumphrey Denit Trust.

[S] The on-line version of this article (available at http://www.jbc.org) contains supplemental Tables S1 and S2.

[1] To whom correspondence should be addressed: 660 W. Redwood St., HH502, Baltimore, MD 21201. Tel.: 410-706-5551; Fax: 410-706-8341; E-mail: mtrudeau@som.umaryland.edu.

[2] The abbreviations used are: LQTS, long QT syndrome; hERG, human *ether-a-go-go*-related gene; I_{Kr}, rapid delayed-rectifier potassium current; PAS, Per-Arnt-Sim; ANOVA, analysis of variance.

we identify a putative "gating face" within the PAS domain, as well as present a general means for rescuing gating-deficient mutant hERG PAS-LQT2 channels.

EXPERIMENTAL PROCEDURES

Molecular Biology and Cell Culture—Unless otherwise noted, hERG PAS-LQT2 mutant constructs were a gift from M. Sanguinetti (University of Utah). hERG K28E, F29L, and M124R were created using the AccuPower HL PCR PreMix (Bioneer). NPAS was created as previously described with amino acids 1–135 directly fused to mCFP at amino acid 135 (15). All hERG constructs, as well as the NPAS fragment, were subcloned into the pcDNA3.1 mammalian expression vector. Human embryonic kidney 293 cells (HEK293) were cultured at 37 °C, 5% CO_2 in Dulbecco's modified Eagle's medium supplemented with 10% fetal bovine serum, 1% penicillin-streptomycin, and 1% L-glutamine. At 50–70% confluence, HEK293 cells were transiently transfected with cDNA using the TransIT-LT1 Transfection Reagent (Mirus) according to the manufacturer's protocol. The cells were incubated for 24–48 h before analysis.

Electrophysiology and Analysis—For electrophysiological recordings, HEK293 cells were plated on 35-mm cell culture dishes and transfected with 1 μg of hERG channel cDNA + 1 μg of NPAS cDNA (or 1 μg mCFP cDNA). Whole cell recordings were performed 24–48 h post-transfection using an EPC-10 patch clamp amplifier (HEKA Instruments). Cells with mCFP fluorescence were chosen for recording, and >90% of cells expressed hERG currents. Data were acquired using PatchMaster Software, version 2.0 (HEKA Instruments), and analyzed using IgorPro Software, version 5.03 (Wavemetrics). All recordings were done at room temperature (22 ± 2 °C) with a sampling rate of 1 kHz unfiltered and a holding potential of −80 mV. Patch pipettes were pulled using a P-97 micropipette puller (Sutter Instruments) and had resistances of 2–4 MΩ when filled with the internal pipette solution. The internal pipette solution contained (in mM): 130 KCl, 1 $MgCl_2$, 5 EGTA, 5 MgATP, and 10 HEPES (pH 7.2 with KOH). The external bath solution contained (in mM): 137 NaCl, 4 KCl, 1.8 $CaCl_2$, 1 $MgCl_2$, 10 glucose, 5 tetraethylammonium, and 10 HEPES (pH 7.4 with NaOH). Series resistance was compensated such that the voltage error was <5 mV. No leak subtraction was used. Currents were measured using either standard voltage step protocols (described in the corresponding figure legends) or a dynamic ramp voltage clamp that mimics the ventricular action potential. Current deactivation was fit with a double exponential function ($y = A_1e^{-t/\tau_1} + A_2e^{-t/\tau_2}$), where t is time and τ is the time constant of deactivation. The current-voltage (IV) relationship was measured by plotting the peak current at the end of the depolarizing pulse normalized to either cellular capacitance (to control for variations in cell size) or the absolute value of the extrapolated maximum peak tail current value elicited by a step from 60 mV to either −50 or −100 mV (indicated in the corresponding figure legend) *versus* voltage. The extrapolated maximum current value was determined from a double exponential fit to the deactivating current extrapolated back to the moment of voltage change, as was done by Sale *et al.* (10). This value represents the maximal conductance and is proportional to the number of open channels. The voltage dependence of activation was measured by plotting the peak tail current *versus* voltage and fit with a Boltzmann function: $y = 1/\{1 + \exp[(V_{½} - V)/k]\}$, where $V_{½}$ is the half-maximal activation potential and k is the slope factor. Steady-state inactivation was measured using a three-pulse protocol, as previously described by Smith *et al.* (25). Errors due to deactivation at −120 and −100 mV were corrected using the following equation: $I_{corrected} = (g_{difference})(20\text{-}E_{rev})$; $g_{difference} = (I_{peak} - I_{end})/(E_{mem} - E_{rev})$, where I_{peak} is the peak current during the 15 ms conditioning pulse, and I_{end} is the current at 15 ms. The resulting values were normalized, plotted *versus* voltage, and fit with a Boltzmann function. Averaged data are presented as mean ± S.E. Statistical analyses were performed using a one-way ANOVA; n represents the number of recordings. For Fig. 1, *A* and *B*, the number of individual transfections per channel type was 2–5, and the number of cells recorded per transfection was 1–3.

Cell Surface Biotinylation Assay—HEK293 cells were plated on 60-mm cell culture dishes and transfected with 1.5 μg of hERG channel cDNA. Approximately 48 h post-transfection, cells were washed twice with ice-cold PBS and then treated with PBS containing 1 mg/ml of EZ-Link Sulfo-NHS-SS-biotin (Pierce) for 30 min at 4 °C. Cells were then incubated with 50 mM Tris (pH 7.5) for 20 min at 4 °C to quench the unreacted biotin, followed by three washes with ice-cold PBS. Following cell lysis (as described below), biotinylated protein was recovered by incubating the cell lysates with neutravidin-coated agarose beads (Pierce) in PBS buffer containing 0.1% SDS for 2 h at 4 °C. Beads were then washed 5 times with PBS plus 0.1% SDS. Biotinylated proteins were eluted from the beads in 2× LSB + β-mercaptoethanol (Bio-Rad) at 65 °C for 5 min. Eluted proteins were resolved by 7.5% SDS-PAGE and Western blot analysis.

Cell Lysis and Western Blot Analysis—Cells were homogenized and lysed in lysis buffer (in mM: 150 NaCl, 25 Tris-HCl (pH 7.4), 20 NaEDTA, 10 NaEGTA, 5 glucose, and 1.0% Triton X-100 plus protease inhibitors, 10 μg/ml each) at 4 °C for 30 min while rotating. Lysates were cleared of debris by centrifugation at 15,000 × g for 15 min at 4 °C. The supernatant was transferred to a clean 1.5-ml microcentrifuge tube, and the protein concentration was quantified using the Bradford assay (Pierce). Protein samples (10–20 μg) were incubated with equal amounts of 2× LSB (Bio-Rad) for 30 min at room temperature, subjected to 7.5% SDS-PAGE, and electrophoretically transferred onto nitrocellulose membranes. The membranes were immunoblotted with an anti-hERG-KA antibody directed against the C terminus, and detected using an ECL detection kit and a ChemiDoc XRS camera (Bio-Rad).

RESULTS

hERG Channels Containing PAS Domain LQT2 Mutations Exhibit a Spectrum of Deficiencies—To characterize functional defects of hERG channels containing LQT2 point mutations in the PAS domain (hERG PAS-LQT2) in a mammalian expression system, we expressed each hERG PAS-LQT2 channel in HEK293 cells. The LQT2 mutations we selected were based on previous findings demonstrating that when point mutations were made at the selected residues, either to a LQT2-associated

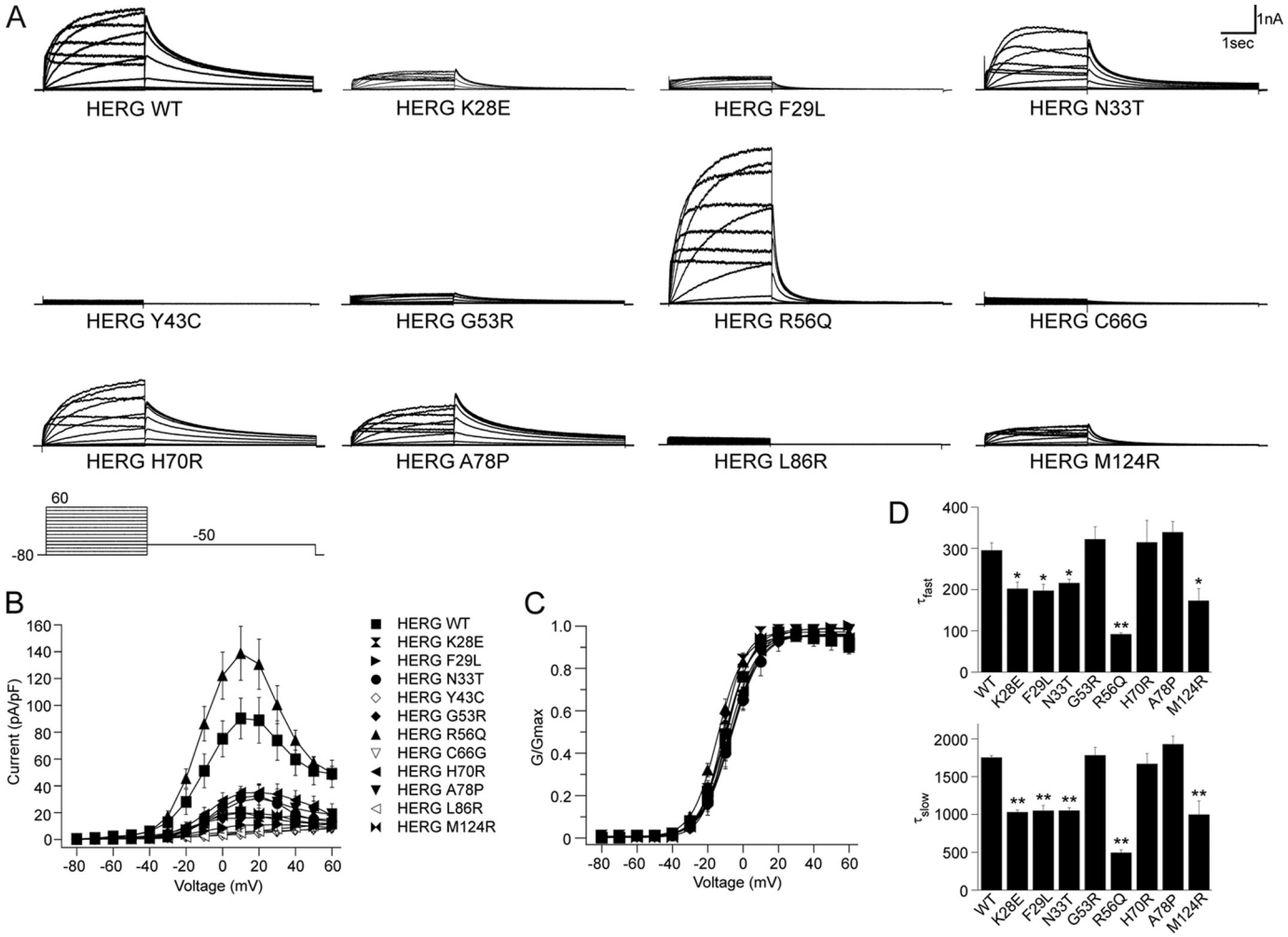

FIGURE 1. **hERG PAS-LQT2 channels exhibit a spectrum of functional defects.** *A*, representative current recordings from HEK293 cells expressing WT or hERG PAS-LQT2 channels. *Inset* represents the voltage command protocol. *B*, IV relationship of WT and each hERG PAS-LQT2 channel. The currents at the end of each depolarizing pulse were normalized to cell capacitance (pF) and plotted *versus* voltage. *C*, steady-state activation plot. Tail current amplitudes during the −50 mV step were normalized to the maximum tail current amplitude and plotted *versus* voltage. Points were fit with a Boltzmann function to yield the $V_{1/2}$ and *k* (slope) values. *D*, histogram of the time constants (τ) of deactivation derived from a double exponential fit of the tail current produced by a step to −50 from 60 mV. *, $p < 0.05$; **, $p < 0.01$ *versus* WT hERG (ANOVA). All values plotted as mean ± S.E.; $n = 3$–9 cells.

mutation or to alanine, the mutant hERG channels exhibited altered deactivation kinetics in *Xenopus* oocytes (6, 13–15). We also included K28E, R56Q, and M124R, which were previously investigated in mammalian cells (22–24). We first measured functional expression of each hERG PAS-LQT2 channel using whole cell patch clamp recordings (Fig. 1). Fig. 1*A* shows representative current recordings from HEK293 cells transiently expressing either wild-type (WT) hERG or one of the hERG PAS-LQT2 channels. From a holding potential of −80mV, cells were depolarized to voltages ranging from −80 to 60 mV in 10-mV increments, followed by a repolarizing step to −50 mV to elicit a tail current. We observed that most of the hERG PAS-LQT2 channels had measurable currents, including K28E, F29L, N33T, G53R, R56Q, H70R, A78P, and M124R, and exhibited inward rectification at more positive potentials, characteristic of WT hERG channels, which produced a bell-shaped IV relationship (Fig. 1, *A* and *B*). The hERG PAS-LQT2 mutant channels Y43C, C66G, and L86R had no measurable hERG current. The steady-state voltage dependence of activation was slightly right-shifted for hERG N33T ($p < 0.05$), whereas the steady-state activation curves for the other mutant channels were not different from that of WT hERG ($p > 0.05$; Fig. 1*C*; see Table 1 and supplemental Table S1).

Because hERG channels with point mutations in the PAS domain had accelerated deactivation kinetics in *Xenopus* oocytes (6, 13–15), we tested whether the rate of deactivation for each hERG PAS-LQT2 channel was similarly faster in mammalian cells. The tail current produced by a step to −50 mV from a potential of 60 mV was fit with a double exponential function to give two time constants of deactivation, τ_{fast} and τ_{slow}. We found that 5 of the 8 hERG PAS-LQT2 channels that expressed functional channels at the cell surface (K28E, F29L, N33T, R56Q, and M124R) had accelerated deactivation kinetics compared with that of WT channels (Fig. 1*D*). Both the fast (τ_f; $p < 0.01$ for R56Q, $p < 0.05$ for the others) and slow (τ_s; $p < 0.01$ for each) components of deactivation were significantly faster for each hERG PAS-LQT2 channel. Of the 5 hERG PAS-LQT2 channels, hERG R56Q had the fastest rate of deactivation compared with that of WT hERG. The average τ_f for WT hERG (ms ± S.E.) was 295 ± 18, compared with 202 ± 16 for K28E,

TABLE 1

Steady-state activation and inactivation properties for hERG WT and each hERG PAS-LQT2 channel

Boltzmann fit values for steady-state activation and inactivation are indicated.

Cell expressing	Activation		Inactivation		
	$V_{1/2}$	k	$V_{1/2}$	k	n
WT	−9.9 ± 1.3	7.0 ± 0.9	−56.7 ± 2.1	−22.4 ± 1.9	5–6
WT + NPAS	−8.5 ± 0.4	7.2 ± 0.4	−57.6 ± 2.3	−23.1 ± 2.1	7
K28E	−12.6 ± 0.8	6.2 ± 0.5	−48.9 ± 2.1	−23.5 ± 1.9	5–6
K28E + NPAS	−15.8 ± 0.5[a]	5.8 ± 0.5	−57.3 ± 2.3	−22.2 ± 2.0	6–7
N33T	−6.4 ± 0.6[a]	8.4 ± 0.5	−45.2 ± 2.1[a]	−26.3 ± 1.9	5–6
N33T + NPAS	−9.6 ± 0.8	7.9 ± 0.6	−55.1 ± 1.9	−22.6 ± 1.7	4–5
R56Q	−13.2 ± 0.7	8.7 ± 0.6	−30.1 ± 2.0[b]	−30.2 ± 1.8	4
R56Q + NPAS	−10.2 ± 0.7	7.7 ± 0.5	−56.1 ± 2.0	−23.5 ± 1.8	6
M124R	−9.9 ± 0.8	6.9 ± 0.5	−43.1 ± 2.0[a]	−25.7 ± 1.8	4
M124R + NPAS	−11.7 ± 1.2	6.4 ± 0.7	−60.9 ± 2.4	−21.9 ± 2.1	4–5

[a] $p < 0.05$ *versus* WT hERG (ANOVA).
[b] $p < 0.01$ *versus* WT hERG (ANOVA).

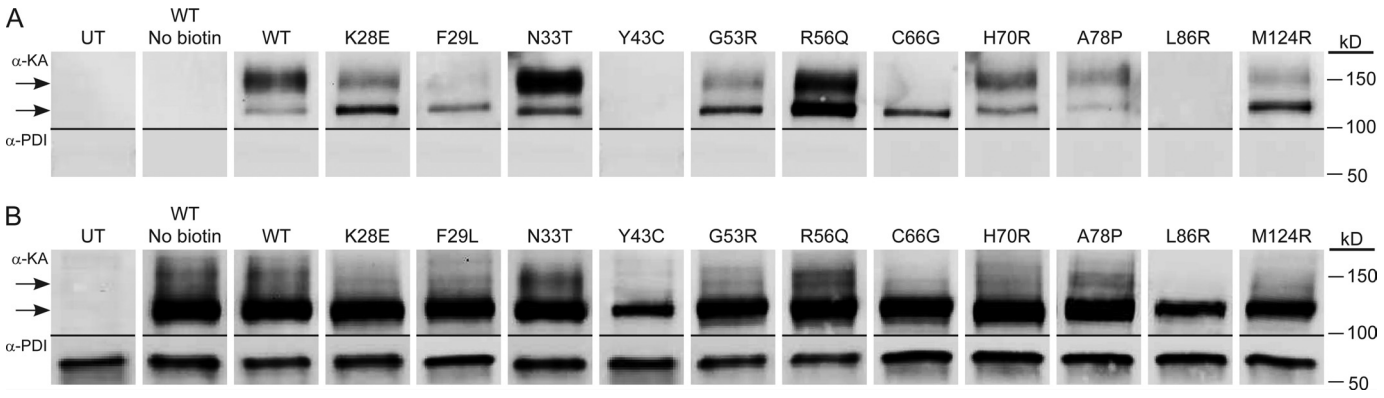

FIGURE 2. **Analysis of cell surface expression of each hERG PAS-LQT2 channel by biotin labeling.** *A*, representative immunoblot of neutravidin-purified biotinylated hERG. Cell surface proteins were biotinylated using the membrane-impermeant form of biotin, sulfo-NHS-SS-biotin, purified with neutravidin beads, and subjected to SDS-PAGE. WT hERG and hERG PAS-LQT2 channels were probed with anti-hERG-KA (*top panels*). The ER-resident protein, protein disulfide isomerase (PDI), was used as a loading control and probed with anti-PDI (*bottom panels*); no PDI was labeled by biotin, confirming biotinylation was specific for surface proteins. No biotinylated protein was purified from untransfected cells (*UT*) or from HEK293 cells expressing WT hERG, but without prior treatment with biotin (*second lane*). *B*, representative immunoblot of whole cell lysates from HEK293 cells following biotinylation treatment. hERG channels were probed with anti-hERG-KA; PDI was probed with anti-PDI as a loading control. Similar results were obtained in three independent experiments.

186 ± 16 for F29L, 216 ± 9 for N33T, 92 ± 3 R56Q, and 173 ± 29 for M124R (Fig. 1*D*, *top panel*); the average τ_s for WT hERG channels (ms ± S.E.) was 1751 ± 25, compared with 1032 ± 29 for K28E, 1060 ± 50 for F29L, 1052 ± 37 for N33T, 495 ± 38 for R56Q, and 999 ± 179 for M124R (Fig. 1*D*, *bottom panel*).

We next asked whether the non-measurable current seen for some of the hERG PAS-LQT2 channels was due to a decrease or lack of protein at the cell surface. To test this, we utilized cell surface biotinylation to measure hERG channels expressed on the plasma membrane. In this assay, hERG channels on the cell surface were biochemically labeled with a membrane-impermeant form of biotin (sulfo-NHS-SS-biotin) and affinity purified with neutravidin beads. WT hERG channels expressed in mammalian cells appear as two bands on a Western blot: one at 155 kDa (representing the mature, complex-glycosylated form; *top arrow* in Fig. 2, *A* and *B*) and one at 135 kDa (representing the immature, core-glycosylated form; *bottom arrow* in Fig. 2, *A* and *B*) (12, 26, 27). In the neutravidin-purified sample, Western blot analysis revealed a robust band for the mature form (Fig. 2*A*, *top arrow*) and a fainter band representing the immature form of WT hERG (Fig. 2*A*, *bottom arrow*), whereas no hERG protein was detected from either untransfected cells or in the absence of biotin. The small amount of the immature protein that we detected is consistent with previous findings where the immature form of hERG was detected using cell surface biotinylation (27, 28). We detected bands representing neutravidin-purified biotinylated hERG from lysates of hERG K28E, F29L, N33T, G53R, R56Q, C66G, H70R, A78P, and M124R, suggesting that these channels were at the cell surface. In contrast, we did not detect protein bands from the neutravidin-purified biotinylated lysates of hERG Y43C and L86R, suggesting a lack of cell surface expression (Fig. 2*A*). We analyzed the total cell lysates from the same samples to verify protein expression for each mutant channel. We detected bands for WT hERG and all of the hERG PAS-LQT2 channels (Fig. 2*B*). As expected, WT hERG channels had robust mature and immature bands on a Western blot. Each hERG PAS-LQT2 channel also had a robust immature band (Fig. 2*B*, *bottom arrow*), but they had varying levels of the mature band (Fig. 2*B*, *top arrow*). For hERG Y43C and L86R, we detected only the immature form of the channel, indicating that these mutant channels undergo only core glycosylation and exhibit defects in protein maturation. Our results from cell surface biotinylation corresponded well with the electrophysiological data. In particular, 1) channels that generated measurable ionic current (WT, K28E, F29L, N33T, G53R, R56Q H70R, A78P, and M124R) also had measurable neutravidin-purified biotinylated hERG protein bands, suggesting expression on the plasma membrane, and 2) channels that had no measurable ionic current (Y43C and L86R) had

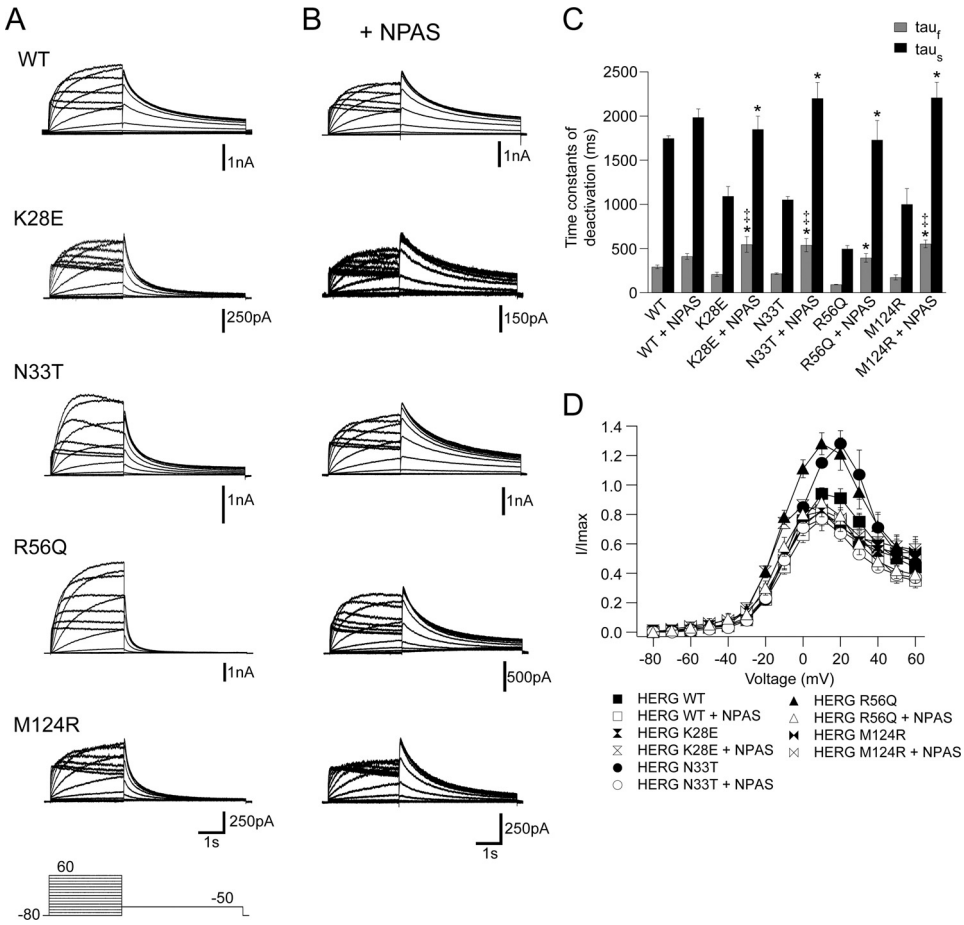

FIGURE 3. **NPAS rescues the gating deficiencies of hERG PAS-LQT2 channels.** Representative current recordings from HEK293 cells expressing WT or hERG PAS-LQT2 channels (*A*) alone and (*B*) with NPAS. *Inset* represents the voltage command protocol used. *C*, histogram of the time constants (τ) of deactivation derived from a double exponential fit to the peak tail current elicited from a step to −50 from 60 mV. *, $p < 0.05$ *versus* hERG PAS-LQT2; ‡, $p < 0.05$ *versus* WT hERG (ANOVA). *D*, IV plot for each hERG channel alone and with NPAS. The current at the end of the depolarizing step was normalized to the extrapolated maximum tail current and plotted *versus* voltage. All values were plotted as mean ± S.E.; $n = 3$–9 cells.

no detectable neutravidin-purified biotinylated hERG protein, suggesting these mutant channels had weak or no expression on the plasma membrane. Although we detected immature hERG C66G in neutravidin-purified biotinylated samples, we did not detect measurable ionic currents, suggesting that immature proteins may have impaired function. Together, our findings show that hERG PAS-LQT2 channels had a variety of dysfunctional maturation and gating properties.

Rescue of Gating-deficient LQT2 Mutant hERG Channels Using NPAS—Previously, we showed that slow deactivation could be restored in mutant hERG channels by application of a genetically encoded PAS domain (NPAS) in *Xenopus* oocytes (15). Here, we asked if NPAS was a general mechanism for rescue by testing: 1) whether NPAS could restore slow deactivation kinetics in gating-deficient hERG PAS-LQT2 channels in a mammalian system and 2) whether NPAS could rescue gating defects in several different mutant channels. Representative current recordings (using the same voltage command protocol as in Fig. 1) are shown in Fig. 3 from HEK293 cells transfected with each gating-deficient hERG PAS-LQT2 channel with (Fig. 3*B*) or without NPAS (Fig. 3*A*). (We attempted to rescue hERG F29L, but the current amplitudes were too small to analyze.) Fits of the tail currents produced by a step to −50 from 60 mV revealed that, for both τ_f and τ_s, NPAS significantly slowed the deactivation kinetics for each hERG PAS-LQT2 channel ($p < 0.05$ for each; Fig. 3*C*). As a negative control, we coexpressed NPAS with WT hERG channels and found no measurable change in the deactivation kinetics in either time constant ($p > 0.05$; Fig. 3, *A*–*C*). Notably, the τ_s values for each hERG PAS-LQT2 channel + NPAS were not different from WT hERG; however, there was a significant increase observed for the τ_f values in hERG K28E, N33T, and M124R ($p < 0.05$). The relative amplitudes of the fast and slow current decays ($A_{fast}/(A_{fast} + A_{slow})$) indicate that the fast component accounted for a greater percentage of the deactivation for each hERG PAS-LQT2 channel (0.5 ± 0.02 for K28E, 0.54 ± 0.02 for N33T, 0.76 ± 0.01 for R56Q, and 0.50 ± 0.03 for M124R) compared with WT hERG (0.40 ± 0.02). Coexpression with NPAS reduced the contribution of the fast component so that the relative amplitude values were more similar to those for WT hERG (0.43 ± 0.04 for K28E, 0.39 ± 0.03 for N33T, 0.41 ± 0.03 for R56Q, and 0.30 ± 0.04 for M124R). Together, these data show that in a mammalian expression system, NPAS restored slow deactivation kinetics in all of the gating-deficient hERG PAS-LQT2 channels.

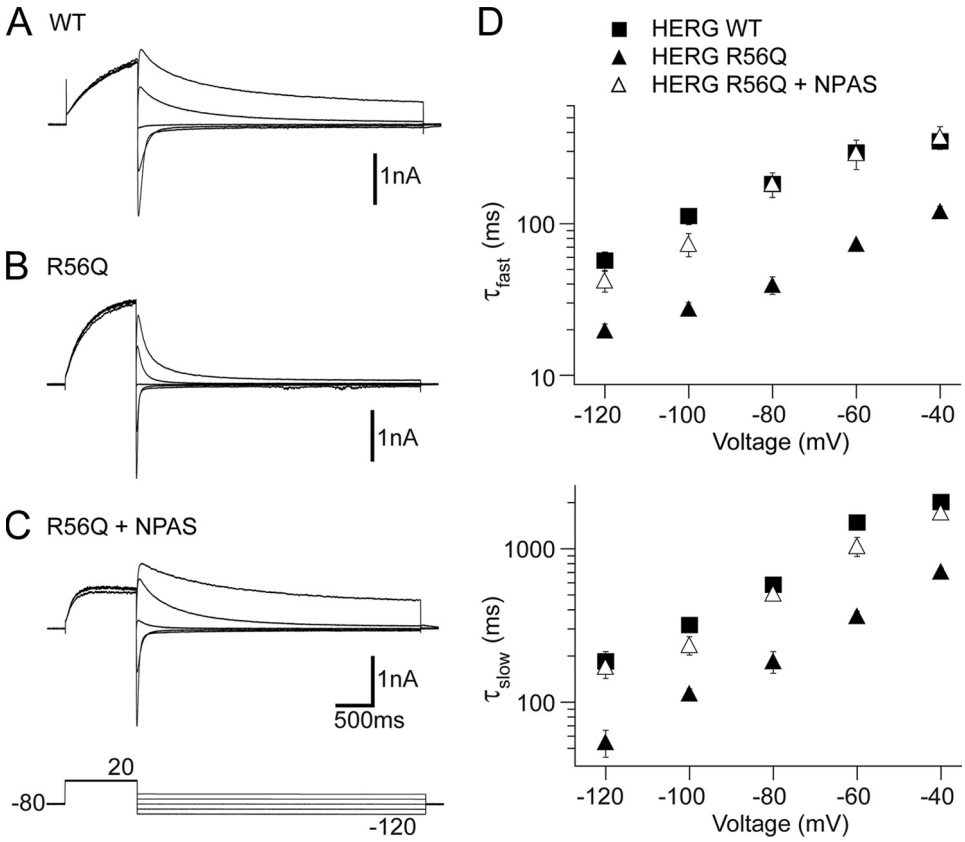

FIGURE 4. **NPAS restores slow deactivation across a range of voltages.** Representative current recordings from: *A,* hERG WT; *B,* hERG R56Q; and *C,* hERG R56Q + NPAS. *Inset* represents the voltage command protocol used. *D*, tails were fit with a double exponential function, and the mean τ_f (*top*) and τ_s (*bottom*) values were plotted against voltage on a logarithmic scale. All values are given as mean ± S.E.; $n = 5–7$ cells.

We next measured the current-voltage (IV) relationship by normalizing the current at the end of each depolarizing step to the extrapolated maximum tail current value at −50 mV (see "Experimental Procedures") following the step to 60 mV, and plotted these values *versus* voltage (Fig. 3*D*). Both hERG N33T and R56Q had significantly larger current amplitudes and comparably less rectification than WT hERG ($p < 0.05$), whereas rectification for hERG K28E and M124R were not different from that for WT channels. Coexpression with NPAS reduced the current amplitude for both hERG N33T and R56Q such that they were not measurably different from WT hERG, whereas it had no effect on the current amplitude for either hERG K28E or M124R. These data demonstrate that alterations in steady-state voltage-dependent gating in some hERG PAS-LQT2 channels were restored by NPAS.

To further characterize altered deactivation for each hERG PAS-LQT2 channel and examine restoration of WT-like kinetics by NPAS, we utilized a voltage command protocol to elicit a family of deactivating traces (Fig. 4). Following channel activation, tail currents were produced by a series of steps ranging from −120 to −40 mV in 20-mV increments, and were fit with a double exponential function to derive time constants of deactivation for each hERG PAS-LQT2 channel (supplemental Table S2). Representative current recordings of WT hERG, hERG R56Q, and hERG R56Q + NPAS, as well as the corresponding τ_f and τ_s values plotted *versus* voltage, are shown in Fig. 4. hERG R56Q exhibited accelerated deactivation kinetics (smaller τ_f and τ_s compared with WT hERG) across a range of command potentials (Fig. 4, *A*, *B*, and *D*). Coexpression with NPAS restored slow deactivation kinetics (larger τ_f and τ_s) in hERG R56Q channels (Fig. 4, *C* and *D*). We observed a similar trend for each of the other gating-deficient hERG PAS-LQT2 channels (supplemental Table S2). Taken together, our findings show that NPAS restored WT-like deactivation gating properties in gating-deficient hERG PAS-LQT2 mutant channels over a range of membrane voltages.

NPAS Rescues Steady-state Properties—To more thoroughly investigate the altered rectification for some of the hERG PAS-LQT2 channels and the subsequent rescue by NPAS (see Fig. 3), we measured the voltage-dependent steady-state current properties. To measure the steady-state inactivation, we used a three-pulse protocol, as described previously (25). After a long depolarizing pulse to maximally activate the channels, the membrane potential was stepped to various potentials ranging from −120 to 60 mV for 15 ms to allow the channels to recover from inactivation and reach a steady-state level. The relative number of open channels was then determined by measuring the peak instantaneous current obtained by a third pulse to 20 mV (Fig. 5*A*, *arrow*). The normalized values were plotted *versus* voltage and fit with a Boltzmann function (Fig. 5*B*). On the same plots, we show the steady-state activation curves, which were generated by plotting the peak tail current values from Fig. 3 *versus* voltage and fitting with a Boltzmann function. We found that there was a positive shift in the steady-state inactivation curves for each hERG PAS-LQT2 mutant channel compared with WT hERG (Fig. 5*B* and Table 1). hERG R56Q exhib-

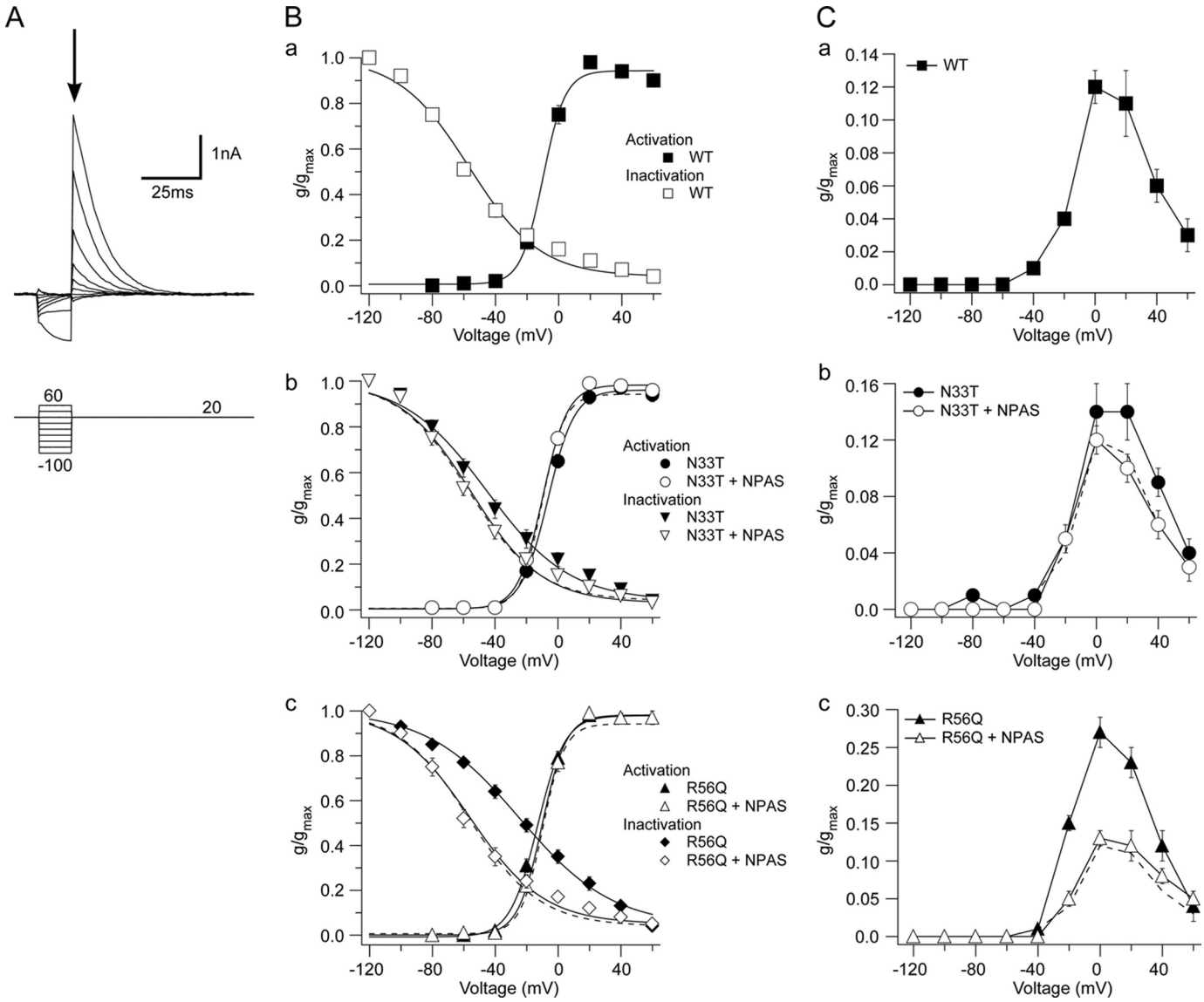

FIGURE 5. **NPAS rescues defects in steady-state properties.** *A*, representative current recording from hERG WT (*top*) using a three-pulse protocol to measure steady-state inactivation (*bottom*). *Large arrow* indicates the peak instantaneous current that was used to generate the steady-state inactivation curve in *B*. *B*, steady-state activation and inactivation plots for: *a*) hERG WT; *b*) hERG N33T; and *c*) hERG R56Q. hERG WT values are shown in the *top plot* and are represented as *dashed lines* in all subsequent plots. Steady-state activation curves were generated using the normalized values of the peak tail current amplitudes from Fig. 3, *A* and *B* and plotted *versus* voltage. Steady-state inactivation curves were generated by plotting the normalized peak instantaneous current (*large arrow*, *A*) *versus* voltage. Both the steady-state activation and inactivation curves were fit with a Boltzmann function. Values are plotted as mean ± S.E.; $n = 4–6$. *C*, the steady-state conductance curves for: *a*) hERG WT; *b*) hERG N33T; and *c*) hERG R56Q. hERG WT values are shown in the *top plot* and are represented as a *dashed line* in all subsequent plots. *Curves* were calculated by multiplying the inactivation and activation curves. Values are plotted as mean ± S.E.; $n = 4–6$ cells.

ited the most profound shift with a $V_{½}$ of −30.1 mV compared with −56.7 mV for hERG WT channels (Fig. 5*B*, *panel c*). Interestingly, coexpression with NPAS restored the steady-state inactivation curves to values that were not different from WT channels (Fig. 5*B* and Table 1), indicating that NPAS regulated hERG channel inactivation. The steady-state activation curves for hERG K28E and N33T were significantly left-shifted when coexpressed with NPAS ($p < 0.05$); the $V_{½}$ and slope factor (k) values for hERG N33T + NPAS were not different from WT hERG ($p > 0.05$; Fig. 5*B*, *panel b*), whereas, the $V_{½}$ for hERG K28E + NPAS was shifted to slightly more negative potentials than WT hERG ($p < 0.05$; Table 1). There was no significant shift for any of the other mutants, which were not different from WT ($p > 0.05$; Table 1). These results show that NPAS restored steady-state inactivation and activation properties of the hERG PAS-LQT2 channels.

We next measured the steady-state conductance-voltage relationship by multiplying the values from the steady-state inactivation and activation curves for hERG N33T and R56Q, which produced a bell-shaped curve (Fig. 5*C*). We observed that for both hERG N33T and R56Q, the peak of the conductance-voltage relationship was larger in amplitude than that for WT hERG, with hERG R56Q ~2-fold larger ($p < 0.05$; Fig. 5*C*, *panel c*). Coexpression with NPAS reduced the peak conductance to values that were similar to those for WT channels. Together, these data demonstrate that the gating-deficient hERG PAS-LQT2 channels exhibited an increase in steady-state channel availability and that

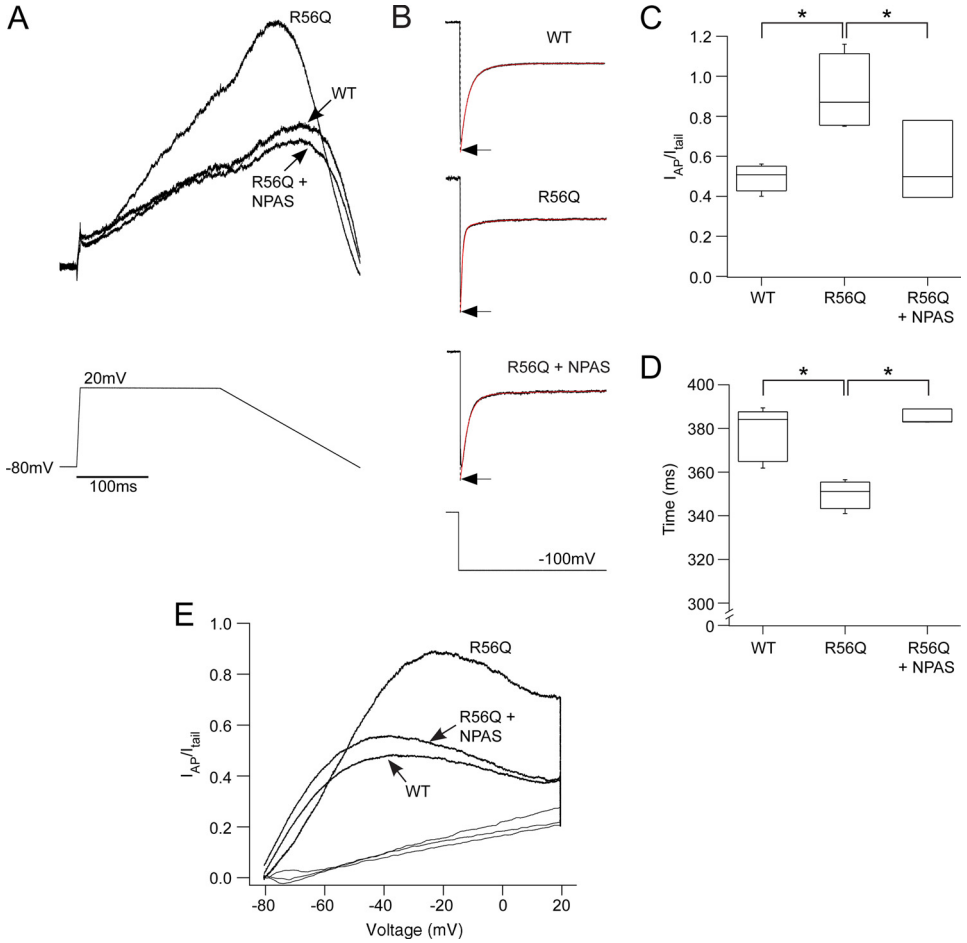

FIGURE 6. **Ionic current generated by hERG WT, hERG R56Q, and hERG R56Q + NPAS in response to a dynamic ramp voltage clamp.** *A*, representative current recordings (*top*) from hERG WT, hERG R56Q, and hERG R56Q + NPAS in response to a dynamic ramp clamp mimicking the ventricular action potential (*bottom*). Currents were normalized to the extrapolated peak tail current elicited at −100 mV (shown in *B*) to account for variations in channel expression between cells. *B*, double exponential fits (*red trace*) of the tail currents generated by a step to −100 from 60 mV extrapolated back to the moment of voltage change to obtain the peak tail current value (*arrow*; see "Experimental Procedures"). *C*, real time IV plot of the currents during the dynamic ramp clamp. *D*, box plot of the peak current generated during the dynamic ramp clamp for hERG WT, hERG, R56Q, and hERG R56Q + NPAS. The *middle line* is the mean, the *top* and *bottom lines* are the 75th and 25th percentiles, respectively, and the *straight lines* are the 90th and 10th percentiles. *E*, box plot of the time (in ms) to the peak current during the dynamic ramp clamp; the *lines* represent the same values as in *D*. *, $p < 0.05$ (ANOVA). Data are plotted as mean ± S.E.; $n = 3–6$ cells.

changes in steady-state properties were restored to WT-like values by NPAS.

NPAS Rescues Altered Resurgent Current Generated by a Dynamic Ramp Voltage Command—Wild-type hERG currents are unusual because the peak current during membrane depolarization is relatively small, but the current resurges and becomes larger during repolarization. We examined the physiological effects of the altered kinetics on resurgent current in hERG PAS-LQT2 channels. To carry out these experiments, we applied a voltage command protocol that mimics the ventricular action potential where, from a holding potential of −80 mV, the membrane potential was stepped to 20 mV with a rise time of 5 ms and held for 200 ms to simulate the plateau phase of the action potential, followed by a gradual decrease in membrane potential to −80 mV over a period of 200 ms (Fig. 6*A*, *bottom*). Similar ramp protocols have previously been used to elicit resurgent currents (14). Because hERG R56Q exhibited the most pronounced alterations in voltage-dependent gating, we chose to investigate this mutant channel using the dynamic ramp. The currents were normalized to the extrapolated peak tail current at −100 mV (shown in Fig. 6*B*; see "Experimental Procedures"). Representative current recordings (Fig. 6*A*, *top*) showed that hERG R56Q generated a larger outward current than WT hERG channels that peaked earlier during the ramp repolarization phase (Fig. 6, *A*, *C*, and *D*, $p < 0.05$), but declined at a faster rate presumably due to its faster deactivation kinetics, similar to what has been previously described (14, 24). We next tested whether NPAS rescued changes in resurgent current. When NPAS was coexpressed with hERG R56Q, the aberrant current was rescued, as the peak outward current and time to peak were shifted to values that were not different from WT hERG (Fig. 6, *A*, *C*, and *D*, $p > 0.05$). Plotting the current-voltage relationship during the dynamic ramp (Fig. 6*E*) further illustrates the shift in the peak current of hERG R56Q to more positive potentials. At more negative potentials, the hERG R56Q current exhibited a rapid decline, and thus, less outward current, whereas the WT hERG current was at its peak. In contrast, coexpression of hERG R56Q with NPAS restored the current-voltage relationship to values that were not different from WT hERG, and shifted the peak current to more negative potentials. These findings demonstrate that NPAS fully restores WT-like current properties of gating-deficient hERG

TABLE 2
Summary of expression of hERG PAS-LQT2 channels and functional rescue by NPAS in HEK293 cells

LQT2	Biogenesis		Surface biotinylation	Ionic current	Altered kinetics	Rescue by NPAS	Gating face
	Immature	Mature					
WT	+++[a]	+++	Y[b]	Y	N	n/a[c]	n/a
K28E	+++	+	Y	Y	Y	Y	Y
F29L	+++	+	Y	Y	Y	N	Y
N33T	+++	+++	Y	Y	Y	Y	Y
Y43C	+	−[d]	N	N	n/a	n/a	Y
G53R	+++	+	Y	Y	N	n/a	N
R56Q	+++	++	Y	Y	Y	Y	Y
C66G	+++	+	Y	N	n/a	n/a	N
H70R	+++	++	Y	Y	N	n/a	N
A78P	+++	++	Y	Y	N	n/a	N
L86R	+++	−	N	N	n/a	n/a	N
M124R	+++	+	Y	Y	Y	Y	Y

[a] + indicates the degree of detection of the tested property.
[b] Y = yes; N = no.
[c] n/a, not applicable.
[d] Minus indicates an absence of the tested property.

PAS-LQT2 channels during a dynamic clamp that mimics a ventricular action potential waveform.

DISCUSSION

In this study, we investigated hERG channels bearing LQT2 mutations in the PAS domain (hERG PAS-LQT2) in a mammalian expression system. Our findings demonstrated that hERG PAS-LQT2 channels exhibited a spectrum of biochemical and functional defects (summarized in Table 2). Most hERG PAS-LQT2 channels (K28E, F29L, N33T, G53R, R56Q, H70R, A78P, and M124R) formed functional ion channels at the cell surface because they exhibited neutravidin-purified biotinylated bands on a Western blot and ionic currents as measured with whole cell patch clamp recordings. Two of the mutant channels (Y43C and L86R) did not have measurable ionic currents or measurable neutravidin-purified biotinylated bands. Instead, these channels had a band on a Western blot of whole cell lysates that corresponded to the immature form of hERG, indicating that these mutant channels most likely had defects in protein maturation. One mutant channel (C66G) had no measurable ionic current and only a faint mature band on a Western blot, but did show an immature band on blots of neutravidin-purified biotinylated samples. We propose that the immature form of hERG may be localized at the plasma membrane in these conditions but that these channels are non-functional. Our data with hERG C66G and L86R are different from previous reports from oocytes that showed robust currents (14). The most likely explanation for differences in channel expression between oocytes (previous study) and HEK293 cells (this study) is a temperature-sensitive folding defect that is apparent with differences in culture temperature for oocytes (16 °C) *versus* HEK293 cells (37 °C), as described for other hERG LQT2 mutant channels (16, 20, 21, 29).

Here we found that 5 hERG-PAS-LQT2 mutant channels (K28E, F29L, N33T, R56Q, and M124R) exhibited altered gating, including accelerated deactivation kinetics, a positive, rightward shift in the steady-state inactivation curve, and increased steady-state channel availability compared with WT hERG. The largest differences in gating and steady-state properties were seen in hERG R56Q. Also, we found that the resurgent hERG R56Q current was larger during depolarization than WT hERG but was smaller during repolarization, especially at voltages less than −60 mV compared with WT hERG (see Fig. 6*E*). We propose that the shift in time of the resurgent peak current and the smaller resurgent current at hyperpolarized voltages in hERG R56Q (see Fig. 6*E*) may be proarrhythmic.

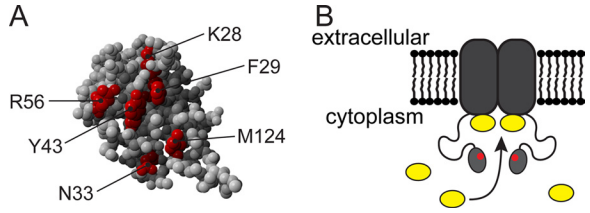

FIGURE 7. **PAS crystal structure and schematic of proposed mechanism of NPAS rescue.** *A*, crystal structure of the hERG PAS domain (6). Residues marked in *red* are all situated on the putative gating face, and LQT2 mutations at these sites, with the exception of Y43C, alter deactivation. *B*, hERG PAS-LQT2 channels that are gating deficient are rescued by NPAS (*yellow*) through replacement of the covalently attached, mutated (red dot) PAS domain.

As the hERG PAS domain is a highly ordered structure, we wanted to know if there was a relationship between the functional defect and the specific location of each LQT2 mutation. We noticed that the LQT2 mutations that altered gating were situated on the same face of the PAS domain (6) (Fig. 7*A*); in contrast, the mutations that either had no effect on kinetics or abolished currents lie elsewhere on the PAS domain. The lone exception to this rule was Y43C, which was also located on the common face but exhibited defects in channel biogenesis. Our data are in agreement with previous work performed with *Xenopus* oocytes in which LQT2 mutations (13, 14) or alanine mutations (6) that affected deactivation were located within a common region of the PAS domain. Previous studies described a hydrophobic patch in the PAS domain, within which lies Phe-29 and Tyr-43, where mutations located in this region caused an increase in the kinetics of deactivation (6). However, because non-hydrophobic sites, especially Arg-56 (15), strongly regulate deactivation, we propose that both hydrophobic and non-hydrophobic residues located nearby one another make up a putative gating face on the PAS domain (Fig. 7*A*), which regulates deactivation and inactivation either allosterically or by forming a direct interaction with another part of the channel, perhaps the C-terminal region (30).

Understanding the molecular defect of each hERG LQT2 channel gives insight into potential mechanisms for restoring WT-like function to mutant channels. To this end, we tested

whether a genetically encoded hERG PAS domain (NPAS) (15) was a general tool to rescue hERG PAS-LQT2 channels in HEK293 cells. We found that NPAS specifically slowed and restored aberrant deactivation gating in hERG PAS-LQT2 channels. We also found that NPAS specifically left-shifted and restored steady-state inactivation gating in the mutant channels and also specifically left-shifted and restored the steady-state activation curve of hERG N33T. NPAS also decreased and restored steady-state channel availability in hERG N33T and R56Q (see Fig. 5*C*). Notably, NPAS fully rescued the defective resurgent current properties of hERG R56Q in response to a dynamic ramp clamp. Our findings demonstrate that NPAS is a general means for rescuing gating-defective hERG LQT2 mutant channels.

In a model we propose to explain the rescue of gating properties by NPAS shown here (Fig. 7*B*), hERG PAS-LQT2 channels exhibit altered deactivation kinetics and steady-state inactivation properties because critical protein interactions between the PAS domain and the channel were disrupted. NPAS physically interacts with the channel and supplants the covalently attached, mutated PAS domain, thus restoring WT-like deactivation kinetics and steady-state inactivation properties. Recently, the notion of using biological alternatives, such as gene therapy, as treatment options for arrhythmogenic diseases like LQT2 was explored (31). Our findings show that NPAS is a useful tool for rescuing gating-deficient mutant hERG channels, and we propose that NPAS may be a potential biological therapeutic for LQT2.

Acknowledgments—We thank Dr. M. Sanguinetti for the hERG PAS-LQT2 cDNAs, Dr. G. Robertson for the anti-hERG-KA antibody, Dr. H. Misono for technical assistance, and Dr. A. Meredith, Dr. J. Montgomery, and A. Gustina for helpful discussions.

REFERENCES

1. Moss, A. J., Schwartz, P. J., Crampton, R. S., Tzivoni, D., Locati, E. H., MacCluer, J., Hall, W. J., Weitkamp, L., Vincent, G. M., Garson, A., Jr., *et al.* (1991) *Circulation* **84,** 1136–1144
2. Warmke, J. W., and Ganetzky, B. (1994) *Proc. Natl. Acad. Sci. U.S.A.* **91,** 3438–3442
3. Trudeau, M. C., Warmke, J. W., Ganetzky, B., and Robertson, G. A. (1995) *Science* **269,** 92–95
4. Sanguinetti, M. C., Jiang, C., Curran, M. E., and Keating, M. T. (1995) *Cell* **81,** 299–307
5. Curran, M. E., Splawski, I., Timothy, K. W., Vincent, G. M., Green, E. D., and Keating, M. T. (1995) *Cell* **80,** 795–803
6. Morais Cabral, J. H., Lee, A., Cohen, S. L., Chait, B. T., Li, M., and Mackinnon, R. (1998) *Cell* **95,** 649–655
7. Wang, J., Trudeau, M. C., Zappia, A. M., and Robertson, G. A. (1998) *J. Gen. Physiol.* **112,** 637–647
8. Viloria, C. G., Barros, F., Giráldez, T., Gómez-Varela, D., and de la Peña, P. (2000) *Biophys. J.* **79,** 231–246
9. Wang, J., Myers, C. D., and Robertson, G. A. (2000) *J. Gen. Physiol.* **115,** 749–758
10. Sale, H., Wang, J., O'Hara, T. J., Tester, D. J., Phartiyal, P., He, J. Q., Rudy, Y., Ackerman, M. J., and Robertson, G. A. (2008) *Circ. Res.* **103,** e81–95
11. Brunner, M., Peng, X., Liu, G. X., Ren, X. Q., Ziv, O., Choi, B. R., Mathur, R., Hajjiri, M., Odening, K. E., Steinberg, E., Folco, E. J., Pringa, E., Centracchio, J., Macharzina, R. R., Donahay, T., Schofield, L., Rana, N., Kirk, M., Mitchell, G. F., Poppas, A., Zehender, M., and Koren, G. (2008) *J. Clin. Invest.* **118,** 2246–2259
12. Zhou, Z., Gong, Q., Epstein, M. L., and January, C. T. (1998) *J. Biol. Chem.* **273,** 21061–21066
13. Al-Owais, M., Bracey, K., and Wray, D. (2009) *Eur. Biophys. J.* **38,** 569–576
14. Chen, J., Zou, A., Splawski, I., Keating, M. T., and Sanguinetti, M. C. (1999) *J. Biol. Chem.* **274,** 10113–10118
15. Gustina, A. S., and Trudeau, M. C. (2009) *Proc. Natl. Acad. Sci. U.S.A.* **106,** 13082–13087
16. Furutani, M., Trudeau, M. C., Hagiwara, N., Seki, A., Gong, Q., Zhou, Z., Imamura, S., Nagashima, H., Kasanuki, H., Takao, A., Momma, K., January, C. T., Robertson, G. A., and Matsuoka, R. (1999) *Circulation* **99,** 2290–2294
17. Ficker, E., Dennis, A. T., Obejero-Paz, C. A., Castaldo, P., Taglialatela, M., and Brown, A. M. (2000) *J. Mol. Cell Cardiol.* **32,** 2327–2337
18. Kagan, A., Yu, Z., Fishman, G. I., and McDonald, T. V. (2000) *J. Biol. Chem.* **275,** 11241–11248
19. Roti Roti, E. C., Myers, C. D., Ayers, R. A., Boatman, D. E., Delfosse, S. A., Chan, E. K., Ackerman, M. J., January, C. T., and Robertson, G. A. (2002) *J. Biol. Chem.* **277,** 47779–47785
20. Anderson, C. L., Delisle, B. P., Anson, B. D., Kilby, J. A., Will, M. L., Tester, D. J., Gong, Q., Zhou, Z., Ackerman, M. J., and January, C. T. (2006) *Circulation* **113,** 365–373
21. Paulussen, A., Raes, A., Matthijs, G., Snyders, D. J., Cohen, N., and Aerssens, J. (2002) *J. Biol. Chem.* **277,** 48610–48616
22. Rossenbacker, T., Mubagwa, K., Jongbloed, R. J., Vereecke, J., Devriendt, K., Gewillig, M., Carmeliet, E., Collen, D., Heidbüchel, H., and Carmeliet, P. (2005) *Circulation* **111,** 961–968
23. Shushi, L., Kerem, B., Goldmit, M., Peretz, A., Attali, B., Medina, A., Towbin, J. A., Kurokawa, J., Kass, R. S., and Benhorin, J. (2005) *Ann. Noninvasive Electrocardiol.* **10,** 334–341
24. Berecki, G., Zegers, J. G., Verkerk, A. O., Bhuiyan, Z. A., de Jonge, B., Veldkamp, M. W., Wilders, R., and van Ginneken, A. C. (2005) *Biophys. J.* **88,** 566–578
25. Smith, P. L., Baukrowitz, T., and Yellen, G. (1996) *Nature* **379,** 833–836
26. Zhou, Z., Gong, Q., Ye, B., Fan, Z., Makielski, J. C., Robertson, G. A., and January, C. T. (1998) *Biophys. J.* **74,** 230–241
27. Gong, Q., Anderson, C. L., January, C. T., and Zhou, Z. (2002) *Am. J. Physiol. Heart Circ. Physiol.* **283,** H77–84
28. Grilo, L. S., Pruvot, E., Grobéty, M., Castella, V., Fellmann, F., and Abriel, H. (2010) *Heart Rhythm* **7,** 260–265
29. Zhou, Z., Gong, Q., and January, C. T. (1999) *J. Biol. Chem.* **274,** 31123–31126
30. Gustina, A. S., and Trudeau, M. C. (2011) *J. Gen. Physiol.* **137,** 315–325
31. Cho, H. C., and Marbán, E. (2010) *Circ. Res.* **106,** 674–685